

Bisphosphonate Functionalized Gadolinium Oxide Nanoparticles Allow Long-Term MRI/CT Multimodal Imaging of Calcium Phosphate Bone Cement

Simone Mastrogiacomo, Alicja E. Kownacka, Weiqiang Dou, Benjamin P. Burke, Rafael T. M. de Rosales, Arend Heerschap, John A. Jansen, Stephen J. Archibald,* and X. Frank Walboomers*

Direct in vivo monitoring of bioconstructs using noninvasive imaging modalities such as magnetic resonance imaging (MRI) or computed tomography (CT) is not possible for many materials. Calcium phosphate-based composites (CPCs) that are applicable to bone regeneration are an example where the materials have poor MRI and CT contrast; hence, they are challenging to detect in vivo. In this study, a CPC construct is designed with gadolinium-oxide nanoparticles incorporated to act as an MRI/CT multimodal contrast agent. The gadolinium(III) oxide nanoparticles are synthesized via the polyol method and surface functionalized with a bisphosphonate (BP) derivative to give a construct (gadolinium-based contrast agents (GBCAs)-BP) with strong affinity toward calcium phosphate. The CPC-GBCAs-BP functional material is longitudinally monitored after in vivo implantation in a condyle defect rat model. The synthetic method developed produces nanoparticles that are stable in aqueous solution (hydrodynamic diameter 70 nm) with significant T_1 and T_2 relaxivity demonstrated in both clinical 3 T and preclinical 11.7 T MRI systems. The combination of GBCAs-BP nanoparticles with CPC gives an injectable material with handling properties that are suitable for clinical applications. The BP functionalization prolongs the residence of the contrast agent within the CPC to allow long-term follow-up imaging studies. The useful contrast agent properties combined with biological compatibility indicate further investigation of the novel bone substitute hybrid material toward clinical application.

In the field of tissue engineering (TE) and regenerative medicine (RM), biological constructs have reached such a high similarity with native tissues that conventional imaging techniques tend to be inadequate for their detection.^[1] However, it is of key importance to be able to monitor the performance of the material over the course of an in vivo trial. Therefore, there is a pressing need for the development of innovative noninvasive imaging approaches, for example, based on multimodal imaging strategies combining magnetic resonance imaging (MRI) and computed tomography (CT).^[2] For example, calcium phosphate-derived cements (CPCs)—a class of advanced injectable and biodegradable bone substitutes—show such high structural similarity with the mineral phase of mammalian osseous tissue that their detection is hampered.^[3] On conventional radiographs, CPC has similar radiopacity to cortical bone and a slightly more radiodense appearance than the surrounding trabecular bone, making the monitoring of the material performance over clinically relevant periods both problematic and inaccurate.^[4]

Dr. S. Mastrogiacomo, Prof. J. A. Jansen, Dr. X. F. Walboomers
Department of Biomaterials
Radboud University Medical Center
P.O. Box 9101, 6500 HB Nijmegen, The Netherlands
E-mail: frank.walboomers@radboudumc.nl

Dr. A. E. Kownacka, Dr. B. P. Burke, Prof. S. J. Archibald
Department of Chemistry
University of Hull
Cottingham Road, HU6 7RX Hull, UK
E-mail: S.J.Archibald@hull.ac.uk

 The ORCID identification number(s) for the author(s) of this article can be found under <https://doi.org/10.1002/adhm.201800202>.

© 2019 The Authors. Published by WILEY-VCH Verlag GmbH & Co. KGaA, Weinheim. This is an open access article under the terms of the Creative Commons Attribution License, which permits use, distribution and reproduction in any medium, provided the original work is properly cited.

The copyright line for this article was changed on 16 September 2019 after original online publication.

DOI: 10.1002/adhm.201800202

Dr. W. Dou
Department of Radiology and Nuclear Medicine
Radboud University Medical Center
Geert Grooteplein Zuid 10, 6525 GA Nijmegen, The Netherlands

Dr. W. Dou
GE Healthcare MR Research China
Beijing 100176, China

Dr. R. T. M. de Rosales
School of Biomedical Engineering & Imaging Sciences
King's College London
London SE1 7EH, UK

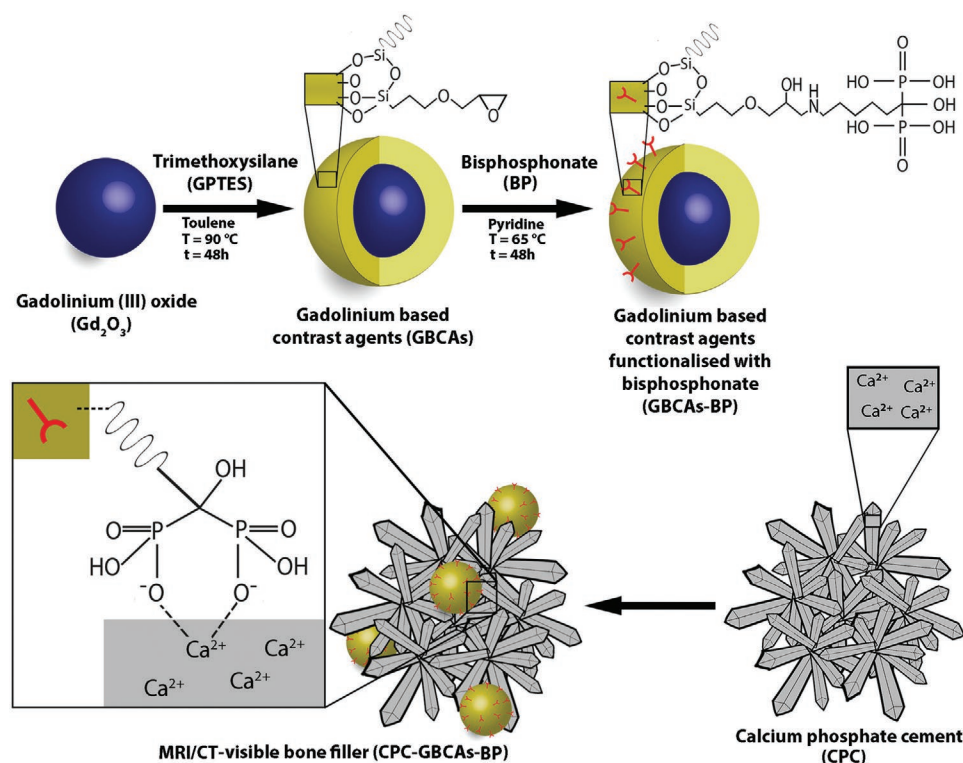
Prof. A. Heerschap
Department of Radiology and Nuclear Medicine
Radboud University Medical Center
Geert Grooteplein Zuid 10, 6525 GA Nijmegen, The Netherlands

The demand for noninvasive imaging modalities makes MRI an ideal technique as it allows noninvasive anatomical imaging and functional 3D visualization of soft tissues with high spatial resolution. Imaging of CPCs using the magnetic resonance (MR) modality can be achieved by application of short or zero echo time acquisition sequences (i.e., ultrashort echo time (UTE) and zero echo time (ZTE), respectively), which acquire data quasi-simultaneously with the excitation pulse. Nevertheless, due to similar transverse relaxation values between cortical bone and CPC (i.e., $T_2 < 1$ ms), the contrast is not sufficient for the material characterization *in vivo*, thus incorporation of additional agent component is required.^[5]

Gadolinium(III) is a lanthanide element with seven unpaired electrons and a symmetric S-state, and it shortens T_1 relaxation times of the water in tissues in which it is taken up, leading to a signal enhancement in T_1 -weighted MRI due to this paramagnetic properties.^[6] Commercially available gadolinium(III)-based contrast agent (GBCAs) have already been utilized to enhance the T_1 signal of CPC constructs *in vivo*.^[7] However, the strategy employed which utilized molecular agents that were not strongly linked to the material showed an insufficient performance level that did not meet the required contrast and longitudinal imaging properties. The CPC degradation profile *in vivo* and the highly porous nature of the material led to leaching of the contrast agent, limiting long-term monitoring properties. Therefore, in order to improve the contrast properties in both CT and MRI the use of gadolinium(III) nanoparticles (NPs) versus molecular agents offers more efficient relaxivity, higher effective concentrations, and the potential to more firmly anchor the contrast agent into the material.

Bisphosphonates (BPs) are well known for their bone-targeting properties. Functionalization of pharmaceuticals (e.g., osteoprotegerin) or nanoparticles (e.g., superparamagnetic iron oxide) with BP groups allows them to strongly interact with the hydroxyapatite mineral phase of the bone offering multiple bonding interactions with calcium ions (Ca^{2+}) from each BP component.^[8] These interactions can be used to specifically bind the GBACs into the CPC matrix and prolong the residence of the imaging probe *in situ*, despite the on-going material degradation. To date, the CPC binding and targeting properties of BP remain unexplored.

Thus, in the presented study, we have developed a surface functionalized GBCAs that can be used for long-term noninvasive monitoring of a specific CPC composite (i.e., mix of alpha-tricalcium phosphate, α -TCP, cryo-grinded poly(D,L-lactide-co-glycolide) microparticles, PLGA, and carboxymethylcellulose, CMC, see Experimental Section in the Supporting Information). To this end, gadolinium oxide (Gd_2O_3) nanoparticles (<5 nm in diameter) for multimodal MR/CT imaging were synthesized via the polyol method. Surface functionalization of the nanoparticles to encapsulate them in a mesoporous silica shell by addition of 3-glycidyloxypropyl trimethoxysilane (GPTES) was used to stabilize the system in aqueous media and to facilitate further functionalization with BP derivatives. The presence of the BP groups in the final constructs enhanced the affinity toward the hydroxyapatite, the main component of the CPC composite, and created the CPC-specific contrast agent (Scheme 1). Elemental analysis and IR spectroscopy was used to characterize the BP functionalization of the GBCAs, while *in vitro* binding experiments confirmed



Scheme 1. Schematic illustration of the GBCA-BP synthesis and combination within the CPC. The multidentate bonding interaction between the phosphonate groups from the BP derivative and the calcium ions from the CPC increases the affinity of GBCA-BP to the mineral phase of CPC.

the high affinity of the BP functionalized GBCAs (GBCAs-BP) toward the solid state CPC. After in vitro toxicity tests and characterization of the handling and mechanochemical properties, the obtained CPC-GBCAs nanocomposite was implanted in vivo in a rat model and the behavior of the material was followed by CT and MRI. The dual-modality nanoparticle probe allowed the visualization of the implanted cement for the entire experimental time course of 8 weeks. Finally, histological assessments were performed to investigate the biological effect of the applied material on the surrounding bone tissues and showed no adverse reactions or inhibition of bone formation.

To form contrast agent, gadolinium oxide nanoparticles were coated with a biocompatible stable silica layer that gives high colloidal stability and contains epoxy rings (from GPTES)

which were used to react with the bisphosphonate precursor and functionalize the surface of the GBCAs (Scheme 1).^[9] Elemental analyses (carbon, hydrogen, and nitrogen (CHN) combustion analysis and inductively coupled plasma optical emission spectroscopy, ICP-OES) were performed on the nanoparticles before and after functionalization, showing the chemical modification of the surface of the nanoparticles at each synthetic step (Figure 1). The results from before and after addition of GPTES offered an assessment of the amount of silica polymerized on the nanoparticles surface. Thus, allowing an estimation of the molar amount of epoxide groups available for covalent conjugation with BP derivative. As expected, analysis of the resulted nanoparticles showed a decrease in the percentage of gadolinium(III) and an increase

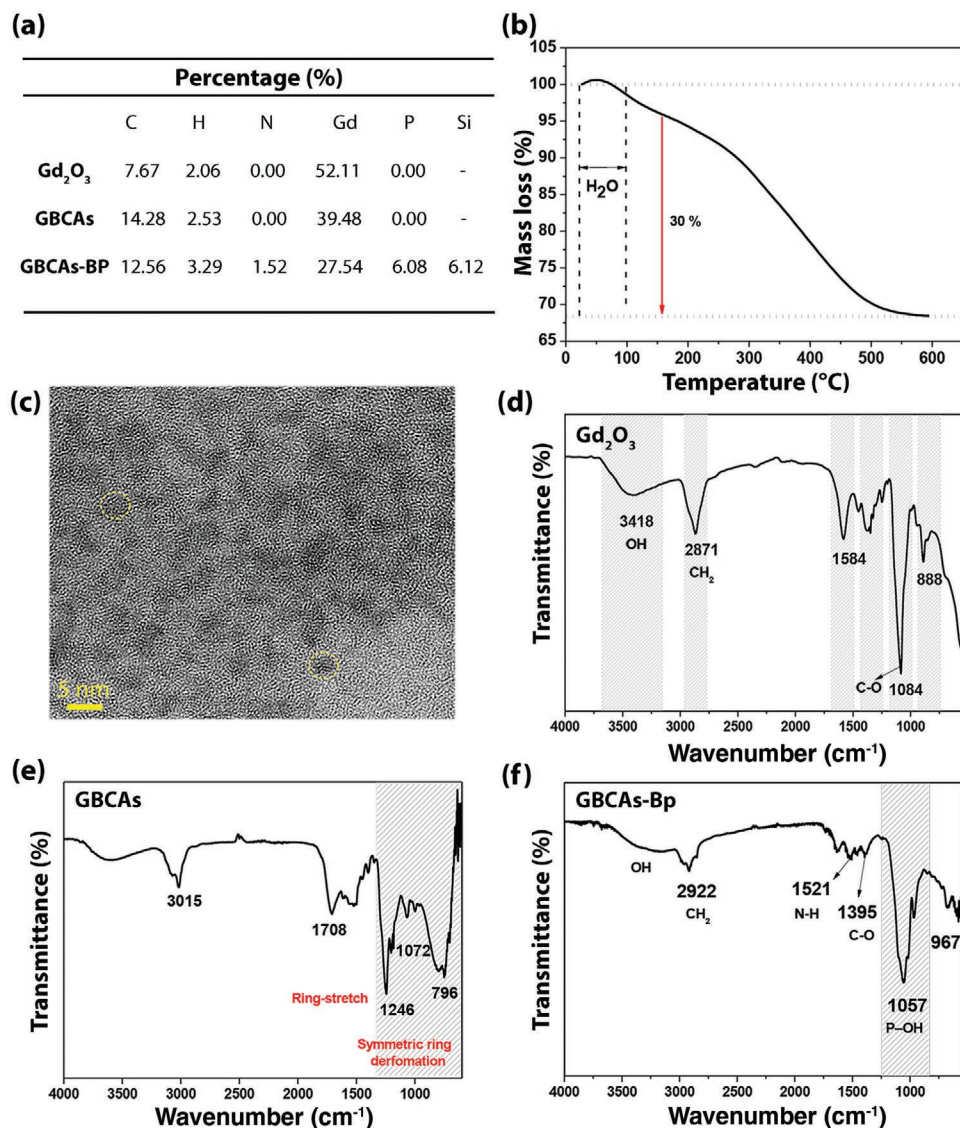


Figure 1. Chemical and morphological characterization of the synthesized nanoparticles. a) Table summarizing the elemental analysis results for the particles after the polyol synthesis, after GPTES stabilization and after BP functionalization, respectively. CHN analysis was performed by combustion using a CHN analyzer, while Gd and P were quantified by ICP-OES. Si content was determined by energy-dispersive X-ray spectroscopy using defined regions of interest from the TEM image. b) TGA analysis of the GBCAs after GPTES coating. c) TEM of GBCAs-BP. Yellow circles define a single particle. d–f) Fourier-transform infrared spectroscopy spectrum of the particles after the polyol synthesis, after GPTES coating, and after BP functionalization, respectively.

of the organic component (Figure 1a). The presence of carbon in the “uncoated” gadolinium oxide sample is due to the diethylene glycol, which is used as a solvent in the reaction as it adsorbs onto nanoparticles surface via interactions with the hydroxyl group stabilizing the NPs in solution.^[10] The detection of nitrogen and phosphorous in the final product (i.e., GBCAs-BP) indicated the presence of the BP derivative on the surface of the nanoparticles. Thermogravimetric analysis (TGA, Figure 1b) was used to assess the overall mass of the organic layer, which was found to be around 30% of the total weight. Transmission electron microscopy (TEM) showed a slight size increase ($\approx 1\text{--}2$ nm) of the Gd_2O_3 nanoparticles core size after GPTES coating, while no differences were observed after BP functionalization (Figure S1, Supporting Information). GBCA-BP nanoparticles were shown to have homogeneous size and morphology with a final core diameter less than 5 nm (Figure 1c), while the measured hydrodynamic diameter was 70 nm. Successful BP functionalization was also confirmed by energy dispersive X-ray spectroscopy (Figure S1, Supporting Information) as well as IR spectroscopy (Figure 1d–f). The IR spectrum of the precursor Gd_2O_3 nanoparticles contains a distinctive peak at 2871 cm^{-1} corresponding to the stretching and bending of the methylene chain (CH_2), a sharp band at 1084 cm^{-1} is assigned to the C–O stretch, and the broad peak

at $3100\text{--}3500\text{ cm}^{-1}$ corresponds to the O–H stretch (Figure 1d). After GPTES coating, the symmetric epoxy ring deformation gives an IR peak in the IR at 788 cm^{-1} , while the sharp band at 1248 cm^{-1} is associated with ring stretching vibrations (Figure 1e), matching previous studies of epoxide derivatives.^[9] In the BP functionalized derivative, the appearance of peaks at 1057 and 1521 cm^{-1} corresponds to the phosphonate groups and to the N–H amide bonds respectively, confirming that the BP functionalization had been achieved (Figure 1f). The characterization data for the GBCAs-BP are summarized in Table S1 in the Supporting Information.

An optimal GBCA for clinical applications needs to have high relaxivity showing significantly shortened T_1 relaxation values, which will allow the required signal enhancement to be achieved at a low enough concentration, and to be incorporated into the CPC without significantly disrupting the properties of the material. In vitro relaxivity studies were performed on the gadolinium nanoparticles with measurements at different magnetic field strengths that are typically found in clinical and preclinical settings (using 3T clinical scanner and 11.7T small bore system across a range of concentrations) (Figure 2 and Table S2, Supporting Information). Increasing the magnetic field strength is known to reduce T_1 relaxivity for gadolinium(III) agents and, in many cases, increase the T_2 relaxivity.^[11]

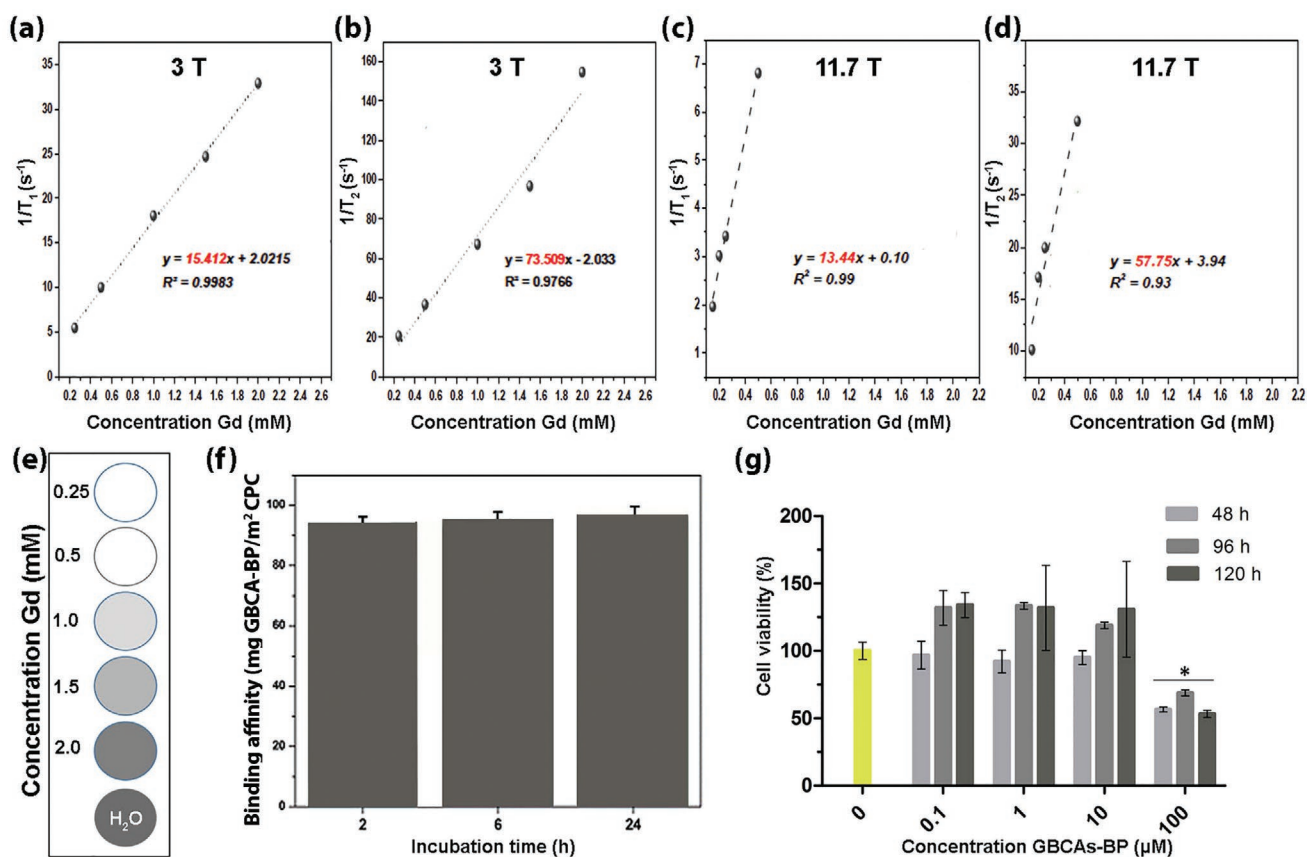


Figure 2. Characterization of the relaxation properties of the particles, their affinity toward the CPC mineral phase, and in vitro cytotoxicity. a,b) plot of $1/T_1$ and $1/T_2$ measured at 3 T, c,d) plot of $1/T_1$ and $1/T_2$ measured at 11.7 T as a function of GBCAs-BP concentration, respectively. r_1 and r_2 were calculated from the slope ($n = 3$). e) The T_1 -weighted MR images of a phantom with GBCAs-BP are shown at different concentrations (image recorded simultaneously). f) The binding profile of GBCAs-BP after 2, 6, and 24 h incubation with CPC cylindrical blocks ($n = 3$). g) Dimethylthiazol-2-yl-5-(3-carboxymethoxyphenyl)-2-(4-sulfophenyl) tetrazolium assay performed on HOB ($n = 3$). * $p < 0.05$. Results are represented as a mean \pm SD. p -values were calculated using one-way analysis of variance (ANOVA) with Tukey’s post hoc test.

To be an effective T_1 contrast agent, the nanoparticles should possess an ultrasmall core size and a hydrophilic coating surface, this ensures that a large surface area of Gd_2O_3 is available to directly interact with the surrounding water molecules and that they can rapidly exchange. Aqueous suspensions of the GBCAs-BP with a concentration of gadolinium(III) varying between 0.2 and 2×10^{-3} M were scanned using inversion recovery for T_1 .^[12] The linear fit of the data acquired versus the concentration of gadolinium(III), gives an overall relaxation rate indicating the efficiency of the contrast agent under the experimental conditions. Specifically, GBCAs-BP showed an r_1 equal to $15.41 \times 10^{-3} \text{ M}^{-1} \text{ s}^{-1}$ at 3 T which is almost four times higher than the commercially available contrast agents (e.g., Magnevist or Omniscan).^[11] Furthermore, the nanoparticles showed only a slight decrease of T_1 relaxivity at 11.7 T, with r_1 equal to $13.44 \times 10^{-3} \text{ M}^{-1} \text{ s}^{-1}$, while the final r_2/r_1 ratio remained similar at the two magnetic field strengths ($r_2/r_1 = 4.77$ at 3 T and $r_2/r_1 = 4.30$ at 11.7 T) (Figure 2a–d and Table S2, Supporting Information). The images of the GBACs-BP phantoms at different concentrations (Figure 2e) show the dominant T_2 effect at higher contrast agent concentrations, indicating that the lower concentrations of GBCAs-BP (i.e., 1.5×10^{-3} M) is effective for a T_1 -weighted signal enhancement, which correlates with appropriate amounts to incorporate into CPC materials. In vitro binding tests demonstrated the high affinity of the GBCAs-BP (>95%) toward the CPC material at up to 24 h incubation time (Figure 2f) with no dissociation observed.

In vitro cytotoxicity studies were performed on primary human osteoblast (HOb) showing a negative effect on cell viability at high concentrations of the GBCAs-BP (i.e., $> 100 \times 10^{-6}$ M, Figure 2g). However, at low concentrations (0.1 , 1 , and 10×10^{-6} M) of the GBCAs-BP showed a beneficial effect on the HOb viability when compared to the nontreated cells (i.e., the internal control) as the nanoparticles induced cell proliferation (Figure 2g). Such findings not only suggested a nontoxic and concentration-dependent effect of the GBCAs-BP nanoparticles, but also highlighted the beneficial potential of the BP functionalization on the cell behavior. This is as expected and in line with the known properties of bisphosphonate compounds, and the role of BP derivatives on the proliferation and differentiation of HOb cells has been investigated.^[13] With this study, we confirm the beneficial effect of BP-coated nanoparticles derivatives on HOb and support further investigation of this strategy for bone regenerative applications.

Once the GBCAs-BP particles were synthesized, characterized, and found to have appropriate properties to enhance contrast in the application, it was important to determine the concentration of the nanoparticle contrast agent that could be added to the CPC composite without affecting its final handling and mechanical properties, and so preliminary studies were carried out (data not shown). Our findings corroborated the reports in the available literature on CPC doping and suggested that adding GBCAs-BP into the CPC composite with a final concentration of 1 wt/wt% would be appropriate. Furthermore, this contrast agent concentration would allow direct comparison with the longitudinal in vivo imaging performances of the CPC-GBCAs-BP construct with the CPC composite doped with a commercial molecular gadolinium(III) contrast that has been described in previous studies.^[7] The handling and mechanical

properties, as well as the imaging features of the prepared CPC-GBCAs-BP nanocomposite, were investigated in vitro (Figure 3). The setting time assessment showed an increase in the initial and final setting profiles for the CPC-GBCAs-BP nanocomposite when compared to the nonlabeled composite (Figure 3a). It is known that by increasing the alendronate concentration in the CPC matrix the setting time increases as a consequence of the coordination interaction between the phosphonate ions and the calcium salts present in the solution, preventing their rapid incorporation into the crystal lattice and hindering the crystal growth and agglomeration.^[14] The internal CPC control consisting of unfunctionalized nanoparticles (i.e., CPC-GBCAs), confirmed the role of the BP groups increasing the setting time of the CPC nanocomposite. However, the setting features observed for the CPC-GBCAs-BP nanocomposite, i.e., initial time of 11 min and final time of 23 min, are still acceptable for clinical use.^[15] The addition of the GBCAs-BP was shown to increase the compressive strength and the E-modulus of the final composite statistically when compared to the nonlabeled cement (Figure 3b,c). The nonfunctionalized control (i.e., CPC-GBCAs) showed no differences in properties when compared to the CPC-GBCAs-BP nanocomposite, suggesting that the mechanical properties were improved by the nanoparticles themselves rather than the BP functionalization on the surface. As measured by Brunauer–Emmett–Teller analysis, the CPC composite consisted of a nanoporous structure (pore width = 18.8 nm, surface area = $9.7 \text{ m}^2 \text{ g}^{-1}$) with a reduction in pore size and surface area observed for the CPC-GBCAs-BP nanocomposite (pore width = 14.3 nm, surface area = $7.4 \text{ m}^2 \text{ g}^{-1}$) possibly suggesting that the added GBCAs-BP were filling these pores to give rise to a more dense microstructure. The final mechanical properties of the CPC-GBCAs-BP were comparable with most of the studied calcium phosphate-based compositions; hence, it is suitable as cancellous bone filler.^[16] Finally, the GBCAs-BP labeled CPC composition showed excellent hydraulic properties as all the pastes could be extruded from the syringe through a 1.7 mm orifice in less than 30 sec by applying a minimal injection force (see Figure 3d).

Gadolinium has a high atomic number ($Z = 64$) and high X-ray attenuation per mass ($3.11 \text{ cm}^2 \text{ g}^{-1}$ at 100 keV) and it has been used as CT contrast agent especially for angiography and aortography applications.^[17] Therefore, the capability of the GBCAs-BP to enhance the CT contrast of the nonlabeled CPC composite was also investigated. Gray value quantification, based on in vitro micro-CT acquisition, reported a shift of the values showing a darkening of the CPC-GBCAs-Bp nanocomposite versus the control (Figure 3e,f). The enhancement of the CT contrast of a calcium phosphate-based composite by using gadolinium-based nanoparticles could offer additional information, especially in cases of a multimodal imaging assessment of the CPC degradation (i.e., using both MRI and CT).

Finally, the MRI properties of the CPC-GBCAs-BP material were investigated after injection in pig bone blocks (Figure 3g) and compared to the nonlabeled CPC. ZTE-MRI acquisitions of the samples containing GBCAs-BP, performed at 11.7 T, showed a typical T_2^* shortening effect which resulted in an imaging artifact that led to a sample size overestimation (Figure 3h). It is known that gadolinium(III) not only has a T_1 -shortening effect, but also a T_2 (T_2^*) shortening effect,

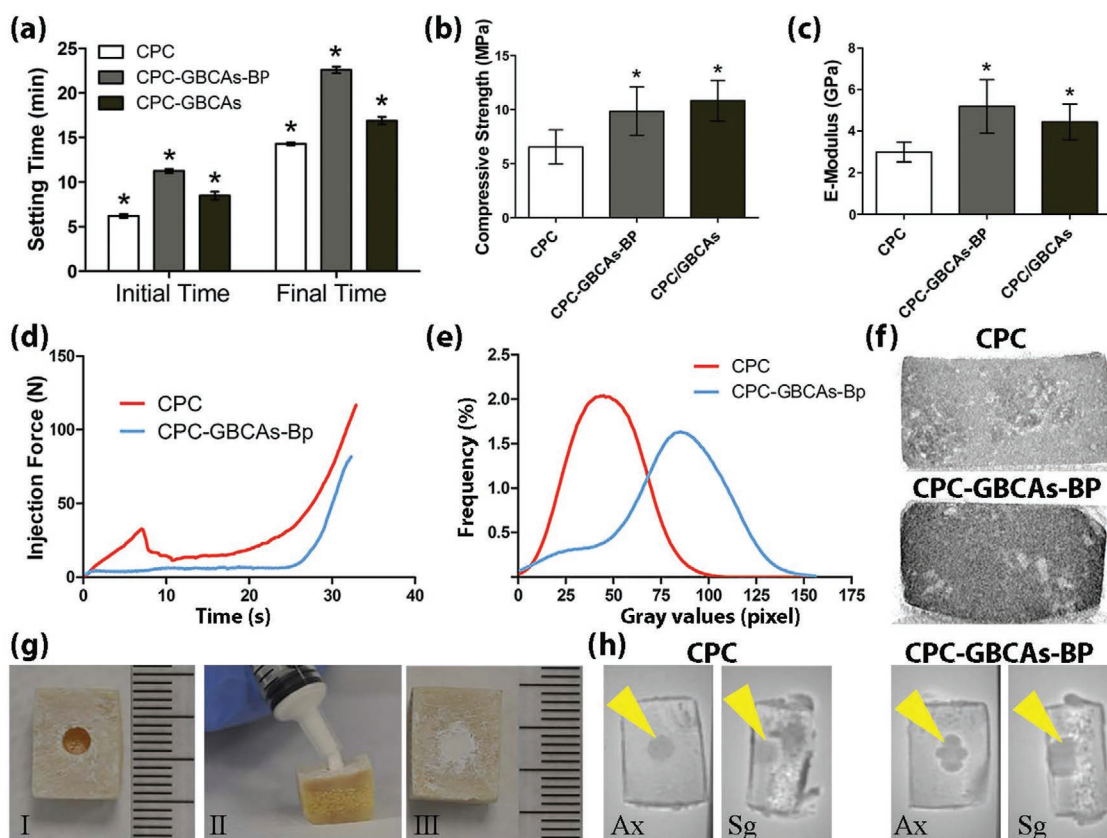


Figure 3. Characterization of the handling and imaging properties of the CPC-GBCAs-BP. a) setting time ($n = 3$), b) compressive strength ($n = 6$), and c) E-modulus ($n = 6$) of the CPC composite without contrast agent, combined with GBCAs and with GBCAs-BP, respectively. d) injectability ($n = 3$) trend of the CPC with and without GBCAs-BP. e) gray value distribution ($n = 3$) of the CPC with and without GBCAs-BP obtained from μ CT assessment (note the pronounced shift to the left from the CPC composition with GBCAs-BP). f) 2D reconstruction of pre-set cylinders of the CPC with (on the top) and without GBCAs-BP (on the bottom) obtained from μ CT acquisition (note the clear visual difference in color of the CPC with and without contrast agent). g–i) Overview of a pig jaw bone block with a cylindrical defect (3×3 mm). g–II—III) CPC with and without GBCAs-BP was used to fill the defect. h) ZTE-MR images of CPC with and without GBCAs-BP after injection in pig bone blocks ($n = 3$). For each sample, the axial and sagittal views are shown respectively (note the shape overestimation caused by the added contrast agent). * $p < 0.05$. Results are represented as a mean \pm SD. p -values were calculated using one-way ANOVA with Tukey's post hoc test.

depending on its concentration.^[18] Qualitative comparison of our results with previous studies where the CPC was combined with commercially available molecular gadolinium(III) agents (i.e., Gd-DTPA/MagneVist) the GBCA-BP nanoparticles showed enhanced contrast with a higher signal intensity, confirming the superior imaging performance of our nanoparticles.^[7] The contrast of CPC without nanoparticles supplementation can be qualitatively observed; however, it has been already proved to be insufficient for in vivo translation (Figure 3h).

To assess the longitudinal MRI and CT imaging behavior of the CPC-GBCAs-BP nanocomposite, an in vivo study was performed (Figure S2, Supporting Information). Respectively, labeled and nonlabeled CPCs were injected in a cylindrical defect prepared in a rat condyle, which is a well-established nonload bearing model commonly used for testing biomaterials.^[19] MRI and CT acquisitions were performed postsurgery (i.e., day 0), and at 4 and 8 weeks with the data shown in Figure 4. After the surgeries, high-resolution ZTE images of the CPC-GBCAs-BP showed a T_2 weighted signal, which resulted in an implant size overestimation (Figure 4a). In contrast, the CPC composite without contrast agent appeared as a dark hypodense region on

ZTE MR images. Such findings were in line with our in vitro assessments (Figure 3h). Longitudinal monitoring showed the superior imaging performances of the CPC-GBCAs-BP compared to the nonlabeled CPC as in the former case it was possible to clearly identify the implanted material at every time point. Moreover, at 4 weeks postsurgery, the implant size of the CPC-GBCAs-BP nanocomposite was observed to have slightly decreased, while in the center of the implant a brighter area appeared. Interestingly, the relative intensity of this bright region increased at 8 weeks (Figure 4a). It is known that GBCAs can lead to a competitive behavior between T_1 and T_2 shortening effects resulting in a bright or dark signal respectively.^[20] Such a competitive effect may explain the appearance of the brighter region in the central part of the implant, although variations in agent concentration could also be an important factor determining the change in signal intensity.

CT images showed enhanced signal intensity in the case of the CPC/GBCAs-BP nanocomposite when compared either to the nonlabeled CPC or to the natural bone phase. The CT signal enhancement persisted for all of the time points and allowed a facile morphological assessment of the implant shape

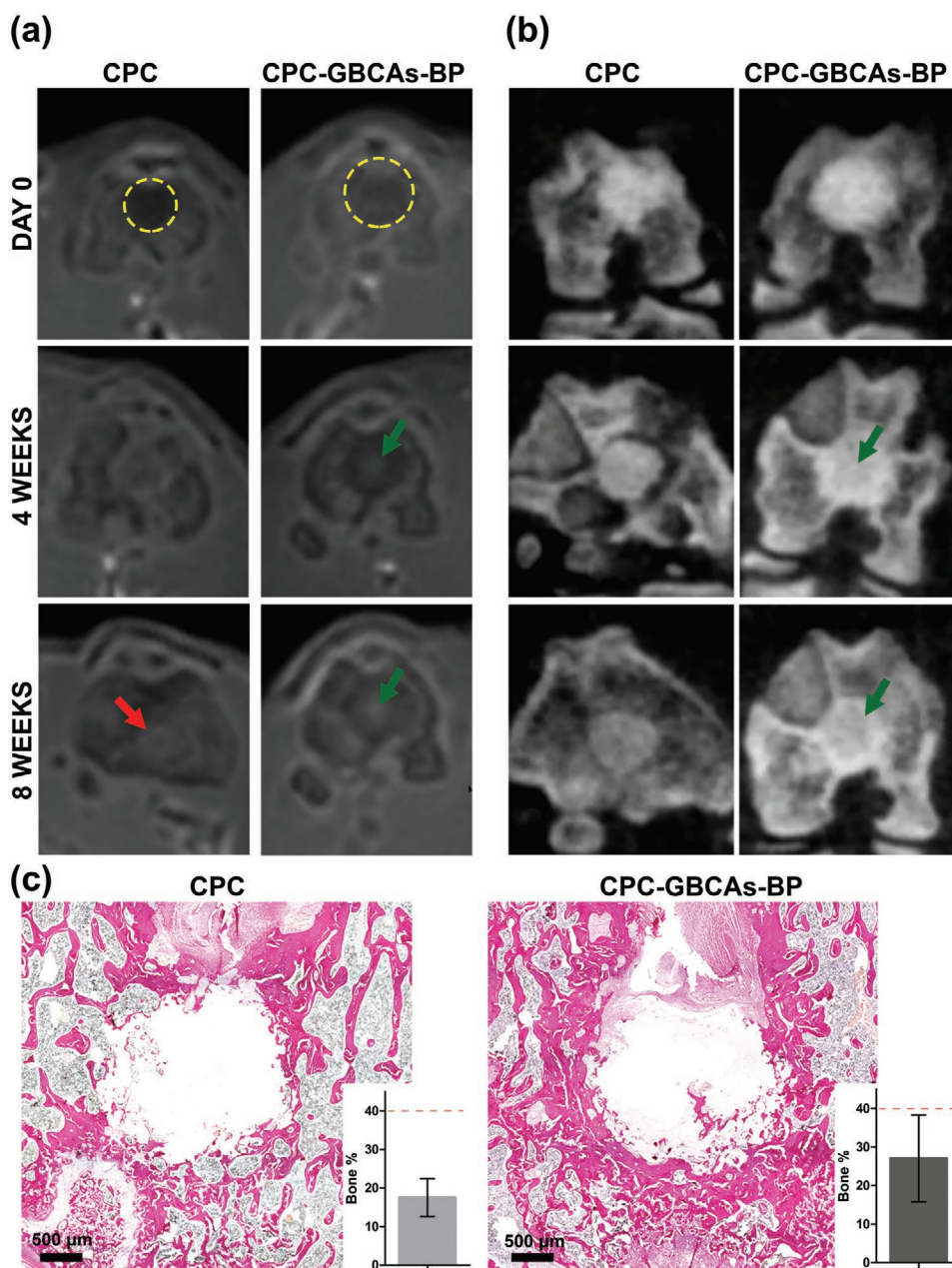


Figure 4. CPC composite with and without GBCAs-BP after injection in a rat condyle defect ($n = 6$). a) The ZTE MR images and b) the CT acquisitions are shown, respectively. From the top to the bottom, the axial view of the same leg after surgery, at 4 and 8 weeks postsurgery are shown, respectively. Note yellow dashed circles that indicate the difference in size between CPC with and without GBCAs-BP. Green arrows indicate the bright region that appears in the middle of the implant on the MRI acquisitions after 4 weeks from the surgery. The bright region corresponds on the CT images to a less dense material. Red arrow indicates the CPC that become indistinguishable from the surrounding bone after 8 weeks from implantation in vivo. c) Histological sections after elastic van gieson staining (scale bar 500 μm). The insets show the new bone formation quantification based on the histological sections. The red dashed lines indicate the bone volume observed in the nontreated samples. Results are represented as a mean \pm SD. p -values were calculated using Student's t -test with Welch's corrections. No significant differences between the groups were found ($p < 0.05$).

and volume (Figure 4b). Interestingly, 4 weeks postsurgery, the CT acquisitions of the implanted CPC-GBCAs-BP showed heterogeneity in material density. Specifically, the central part of the implant appeared to be less dense compared to the outer area. Such findings were in line with the MRI acquisitions and confirmed that there is a lower GBCAs-BP concentration in the central part of the CPC composite. Moreover, the comparison

of these findings with longitudinal studies performed in a similar animal model, but with nonfunctionalized contrast agents (i.e., molecular gadolinium(III) agents or superparamagnetic iron oxide particles), proved the feasibility of our strategy in prolonging the residence of the contrast agent in the CPC matrix up to at least 8 weeks postsurgery.^[8,20] One potential issue is the observed implant size overestimation on MR

images; however, this property could be considered an advantage for detection especially when small amounts of the cement need to be identified in the body. For instance, extravertebral CPC extrusion is a common problem after vertebroplasty that causes pain and neurological complications.^[21] In these circumstances, the size-overestimation effect could serve to identify leakage of small amount of cement outside of the surgical site, hence supporting the surgeon in the postoperative neurological examination.

Histological assessment was performed 8 weeks after surgeries and showed a direct contact between bone and the cement, without sign of inflammation or fibrous encapsulation (see Figure 4c and Figure S3, Supporting Information). BP-loaded CPCs have been used to increase bone augmentation after in vivo implantation in femora and vertebra of osteoporotic rats. Specifically, release of BP derivatives from the CPC phase resulted in an increased bone density in the immediate proximity of the implant (i.e., in an area from 0.4 to 0.7 mm far the cement).^[22] Our histological findings were in line with these previous studies indicating higher bone density may be present around the implant when compared to the CPC composition without BP components (Figure 4c). However, statistical t-testing did not show significant differences in new bone formation between the experimental groups of this size and so further studies are necessary to validate this observation (Figure 4c).

One area of further study that is ongoing is to look at the release profile in vivo and the biodistribution of the GBCAs-BP on release from the CPC composite. Methods for radiolabeling are under investigation to determine a valid quantitative tracking. Previous studies have showed that GBCAs do not undergo to intracellular accumulation and are generally excreted by the hepatobiliary or renal systems.^[23] The decrease in MRI and CT signal over time and the absence of background signals in the surrounding tissues indicate that any GBCAs-BP released from the materials did not accumulate and were eliminated from the body. Histological assessments using elemental analysis (e.g., inductively coupled plasma mass spectroscopy (ICP-MS) and inductively coupled plasma atomic emission spectroscopy (ICP-AES)) and TEM on tissue samples from different organs (e.g., kidney, liver, spleen, and brain) can provide useful and unequivocal information regarding the bioaccumulation of the nanoparticles once released from the implanted CPC. Additionally, hemolytic tests to investigate the lysis of erythrocytes in response to the release of the nanoparticles from the CPC in the bloodstream are suggested to further investigate their biocompatibility and potential use for medical applications.^[24]

The overall profile of the ultrasmall Gd₂O₃ nanoparticles that have been designed and produced in this work offers a significant advance over the current state-of-the-art for longitudinal imaging of calcium phosphate cements. The key image acquisition features are effective multiple modality imaging (combining contrast in both MR and CT from a single agent) and high relaxivity across appropriate MR field strengths. A feature of equally high importance for longitudinal studies is the high affinity for the cement material, which is due to the bisphosphonate coating added to the silica layer.

Supporting Information

Supporting Information is available from the Wiley Online Library or from the author.

Acknowledgements

S.M. and A.E.K. contributed equally to this work. S.M., A.E.K., and W.D. received funding from People Programme (Marie Curie Action) of the European Union's Seventh Framework Programme FP7/2007-2013/ under REA grant agreement No. 607868 (iTERM). The authors are grateful for the technical support to Drs. Vincent Cuijpers, Martijn Martens, Natasja van Dijk, Danny Gerrits, Andor Veltien, and Bianca Lammers van der Weem. The animal study was performed after the approval of the Animal Ethics Committee for the care and use of laboratory animals (RU-DEC number 2015-0035) and in agreement with the standards of the Radboud University Medical Center, Nijmegen, the Netherlands.

Conflict of Interest

The authors declare no conflict of interest.

Keywords

biphosphonate, calcium phosphate cements, computed tomography, gadolinium-based contrast agents, magnetic resonance imaging

Received: February 23, 2018

Revised: May 22, 2018

Published online: August 17, 2018

- [1] a) S. Pina, J. M. Oliveira, R. L. Reis, *Adv. Mater.* **2015**, *27*, 1143; b) G. S. Sailaja, P. Ramesh, S. Vellappally, S. Anil, H. K. Varma, *J. Biomed. Sci.* **2016**, *23*, 77.
- [2] a) L. E. Smith, R. Smallwood, S. Macneil, *Microsc. Res. Tech.* **2010**, *73*, 1123; b) A. A. Appel, M. A. Anastasio, J. C. Larson, E. M. Brey, *Biomaterials* **2013**, *34*, 6615; c) S. Y. Nam, L. M. Ricles, L. J. Suggs, S. Y. Emelianov, *Tissue Eng., Part B* **2015**, *21*, 88.
- [3] a) W. Habraken, P. Habibovic, M. Epple, M. Bohner, *Mater. Today* **2016**, *19*, 69; b) J. Zhang, W. Liu, V. Schnitzler, F. Tancret, J.-M. Bouler, *Acta Biomater.* **2014**, *10*, 1035; c) R. O'Neill, H. O. McCarthy, E. Montufar, M. P. Ginebra, D. I. Wilson, A. Lennon, N. Dunne, *Acta Biomater.* **2017**, *50*, 1.
- [4] a) S. Larsson, *J. Orthop. Trauma* **2010**, *24*, S41; b) F. D. Beaman, L. W. Bancroft, J. J. Peterson, M. J. Kransdorf, D. M. Menke, J. K. DeOrio, *Radiographics* **2006**, *26*, 373; c) S. Mastrogiacomo, W. Dou, O. Koshkina, O. C. Boerman, J. A. Jansen, A. Heerschap, M. Srinivas, X. F. Walboomers, *ACS Appl. Mater. Interfaces* **2017**, *9*, 22149.
- [5] a) M. Ventura, O. C. Boerman, C. de Korte, M. Rijpkema, A. Heerschap, E. Oosterwijk, J. A. Jansen, X. F. Walboomers, *Tissue Eng., Part B* **2014**, *20*, 578; b) M. D. Robson, P. D. Gatehouse, M. Bydder, G. M. Bydder, *J. Comput. Assisted Tomogr.* **2003**, *27*, 825; c) J. E. Holmes, G. M. Bydder, *Radiography* **2005**, *11*, 163.
- [6] a) T. J. Fraum, D. R. Ludwig, M. R. Bashir, K. J. Fowler, *J. Magn. Reson. Imaging* **2017**, *46*, 338; b) Z. Zhou, Z. R. Lu, *Wiley Interdiscip. Rev.: Nanomed. Nanobiotechnol.* **2013**, *5*, 1; c) G. Singh, B. H. McDonagh, S. Hak, D. Peddis, S. Bandopadhyay, I. Sandvig, A. Sandvig, W. R. Glomm, *J. Mater. Chem. B* **2017**, *5*, 418.

- [7] Y. Sun, M. Ventura, E. Oosterwijk, J. A. Jansen, X. F. Walboomers, A. Heerschap, *Tissue Eng., Part C* **2013**, *19*, 281.
- [8] a) R. A. Nadar, N. Margiotta, M. Iafisco, J. J. P. van der Beucken, O. C. Boerman, S. C. G. Leeuwenburgh, *Adv. Healthcare Mater.* **2017**, *6*, 8; b) L. E. Cole, T. Vargo-Gogola, R. K. Roeder, *Adv. Drug Delivery Rev.* **2016**, *99*, 12; c) V. Kubicek, J. Rudovsky, J. Kotek, P. Hermann, L. Vander Elst, R. N. Muller, Z. I. Kolar, H. T. Wolterbeek, J. A. Peters, I. Lukes, *J. Am. Chem. Soc.* **2005**, *127*, 16477; d) L. Sandiford, A. Phinikaridou, A. Protti, L. K. Meszaros, X. Cui, Y. Yan, G. Frodsham, P. A. Williamson, N. Gaddum, R. M. Botnar, P. J. Blower, M. A. Green, R. T. de Rosales, *ACS Nano* **2013**, *7*, 500.
- [9] M. Cano, G. de la Cueva-Mendez, *Chem. Commun.* **2015**, *51*, 3620.
- [10] G. Azizian, N. Riyahi-Alam, S. Haghgoo, H. R. Moghimi, R. Zohdiaghdam, B. Rafiei, E. Gorji, *Nanoscale Res. Lett.* **2012**, *7*, 549.
- [11] a) P. Caravan, C. T. Farrar, L. Frullano, R. Uppal, *Contrast Media Mol. Imaging* **2009**, *4*, 89; b) G. E. Hagberg, K. Scheffler, *Contrast Media Mol. Imaging* **2013**, *8*, 456.
- [12] a) J. Fang, P. Chandrasekharan, X. L. Liu, Y. Yang, Y. B. Lv, C. T. Yang, J. Ding, *Biomaterials* **2014**, *35*, 1636; b) H. B. Na, T. Hyeon, *J. Mater. Chem.* **2009**, *19*, 6267; c) A. Louie, *Chem. Rev.* **2010**, *110*, 3146; d) M. Cho, R. Sethi, J. S. Narayanan, S. S. Lee, D. N. Benoit, N. Taheri, P. Decuzzi, V. L. Colvin, *Nanoscale* **2014**, *6*, 13637.
- [13] O. Fromigie, J. J. Body, *J. Endocrinol. Invest.* **2002**, *25*, 539.
- [14] a) Z. Jindong, T. Hai, G. Junchao, W. Bo, B. Li, W. B. Qiang, *Orthopedics* **2010**, *33*, 561; b) S. Bose, S. Tarafder, *Acta Biomater.* **2012**, *8*, 1401; c) L. M. Grover, U. Gbureck, A. M. Young, A. J. Wright, J. E. Barralet, *J. Mater. Chem.* **2005**, *15*, 4955; d) L. M. Grover, A. J. Wright, U. Gbureck, A. Bolarinwa, J. Song, Y. Liu, D. F. Farrar, G. Howling, J. Rose, J. E. Barralet, *Biomaterials* **2013**, *34*, 6631.
- [15] K. L. Low, S. H. Tan, S. H. Zein, J. A. Roether, V. Mourino, A. R. Boccaccini, *J. Biomed. Mater. Res., Part B* **2010**, *94*, 273.
- [16] J. Zhang, W. Liu, V. Schnitzler, F. Tancret, J. M. Bouler, *Acta Biomater.* **2014**, *10*, 1035.
- [17] a) N. Lee, S. H. Choi, T. Hyeon, *Adv. Mater.* **2013**, *25*, 2641; b) J. W. Henson, R. G. Nogueira, D. J. Covarrubias, R. G. Gonzalez, M. H. Lev, *AJNR Am. J. Neuroradiol.* **2004**, *25*, 969; c) S. Chryssidis, R. P. Davies, M. L. Tie, *Australas. Radiol.* **2002**, *46*, 97.
- [18] a) M.-J. Lee, M.-J. Kim, C.-S. Yoon, S. Y. Song, K. Park, W. S. Kim, *Korean J. Radiol.* **2011**, *12*, 358; b) A. T. Tirkes, M. A. Rosen, E. S. Siegelman, *Int. J. Cardiovasc. Imaging* **2003**, *19*, 151; c) M. Kanematsu, M. Matsuo, Y. Shiratori, H. Kondo, H. Hoshi, I. Yasuda, H. Moriwaki, *Am. J. Roentgenol.* **2002**, *178*, 755; d) V. Y. Kuperman, M. T. Alley, *J. Magn. Reson. Imaging* **1999**, *9*, 172.
- [19] M. Bongio, J. J. van den Beucken, S. C. Leeuwenburgh, J. A. Jansen, *J. Tissue Eng. Regen. Med.* **2015**, *9*, 191.
- [20] a) M. Ventura, Y. Sun, V. Rusu, P. Laverman, P. Borm, A. Heerschap, E. Oosterwijk, O. C. Boerman, J. A. Jansen, X. F. Walboomers, *Tissue Eng., Part C* **2013**, *19*, 405; b) M. Ventura, Y. Sun, S. Cremers, P. Borm, Z. T. Birgani, P. Habibovic, A. Heerschap, P. M. van der Kraan, J. A. Jansen, X. F. Walboomers, *Biomaterials* **2014**, *35*, 2227.
- [21] a) M. Nakano, N. Hirano, H. Ishihara, Y. Kawaguchi, K. Matsuura, *J. Neurosurg.* **2005**, *2*, 27; b) X. Wang, J. Ye, Y. Wang, *Acta Biomater.* **2007**, *3*, 757.
- [22] a) E. Verron, O. Gauthier, P. Janvier, P. Pilet, J. Lesoeur, B. Bujoli, J. Guicheux, J. M. Bouler, *Biomaterials* **2010**, *31*, 7776; b) E. Verron, M.-L. Pissonnier, J. Lesoeur, V. Schnitzler, B. H. Fella, H. Pascal-Moussellard, P. Pilet, O. Gauthier, J.-M. Bouler, *Acta Biomater.* **2014**, *10*, 4887.
- [23] a) S. Aime, P. Caravan, *J. Magn. Reson. Imaging* **2009**, *30*, 1259; b) D. Kryza, J. Taleb, M. Janier, L. Marmuse, I. Miladi, P. Bonazza, C. Louis, P. Perriat, S. Roux, O. Tillement, C. Billotey, *Bioconjugate Chem.* **2011**, *22*, 1145.
- [24] a) B. J. Marquis, S. A. Love, K. L. Braun, C. L. Haynes, *Analyst* **2009**, *134*, 425; b) S. A. Love, M. A. Maurer-Jones, J. W. Thompson, Y. S. Lin, C. L. Haynes, *Annu. Rev. Anal. Chem.* **2012**, *5*, 18; c) M. A. Dobrovolskaia, J. D. Clogston, B. W. Neun, J. B. Hall, A. K. Patri, S. E. McNeil, *Nano Lett.* **2008**, *8*, 2180.